Proceedings of the Thirtieth (2020) International Ocean and Polar Engineering Conference **www.isope.org**
Shanghai, China, October 11-16, 2020

ISBN 978-1-880653-84-5; ISSN 1098-6189

Multi-Variable Feedforward Control for Floating Wind Turbines Using Lidar

David Schlipf [1], *Frank Lemmer* [2], *Steffen Raach* [3]
[1] Wind Energy Technology Institute, Flensburg University of Applied Sciences, Flensburg, Germany
[2] Stuttgart Wind Energy, Universität Stuttgart, Stuttgart, Germany
[3] sowento GmbH, Stuttgart, Germany

ABSTRACT

In this work a multi-variable feedforward controller for floating wind turbines is presented. The feedforward controller provides a pitch rate and a torque update to a conventional feedback controller based on a wind speed preview. A 10 MW reference wind turbine is used on a semi submersible floating platform to study the potential of the controller. An open-source simulation tool is extended with an realistic lidar simulator and the lidar data processing, feedforward controller, and feedback controller are implemented in modular setup. The lidar measurements are fully motion compensated and combined to provide a preview of the rotor-effective wind speed to the controller. The feedforward controller is designed to minimize structural loads and to decrease the platform pitch motion. In verification and simulation studies the concept is demonstrated and the multi-variable feedforward controller shows a promising improvement in speed regulation and load reduction on the floating wind turbine.

KEYWORDS

floating wind turbine control; feedforward control; lidar-assisted control; smart lidar; reduced order modeling.

INTRODUCTION

Lidar-assisted control is a promising technology to reduce structural loads and increase energy production for wind turbines. The technology has proven its capability to improve control performance for onshore wind turbines in field tests. The impact on floating offshore turbines (FOWTs) is even more promising, since their dynamics depend heavily on the aerodynamic thrust, see Schlipf et al. (2015b). Nonlinear Model Predictive Controller (NMPC) with lidar wind preview was applied to a 5 MW wind turbine by Schlipf et al. (2013) and Raach et al. (2014b). Also, a collective pitch feedforward controller was optimized for FOWTs by Schlipf et al. (2015b) to cancel out the impact of wind speed changes to the aerodynamic torque. Wave preview was subject of different works with the aim of canceling wave forcing through the knowledge of the incoming wave field. A state-space wave force model was developed in Lemmer et al. (2016a) in order to model the Froude-Krylov forces in real time based on the instantaneous free-surface elevation. The question of how to design a wave feedforward controller was addressed recently by Al (2019).

In this paper, we present a multi-variable feedforward controller for floating offshore wind turbines (FOWTs), providing not only a pitch rate update but also a generator torque update to a conventional feedback controller based on a wind speed preview and thus not only canceling the impact of wind speed changes on the aerodynamic torque, but to the aerodynamic thrust as well. The present work aims at showing the potential of combining existing lidar feedforward techniques to FOWTs: A standardized DLL-chain that is directly applicable on commercial wind turbine systems are used in this work and simulated for a 10 MW FOWT. The paper starts with a description of the general objectives. Then, the numerical modeling and lidar data processing are presented. After that, the controller design methodology is introduced and the simulation results are shown and discussed.

OBJECTIVES

The main objective of the paper is to demonstrate the potential of lidar-assisted control for floating wind turbines by the design of a multi-variable feedforward controller, providing signals for pitch and torque actuator. The collective pitch feedforward rate is designed to compensate the impact of the rotor effective wind speed (REWS) on the aerodynamic thrust and thus reduces the tower and platform pitch motion. The generator torque update is then designed compensating the impact of the rotor effective wind speed and the collective pitch angle on the aerodynamic torque and thus reduces the rotor motion. We use the SWE-TripleSpar floating platform (Lemmer et al. (2020a)) with the DTU 10 MW reference wind turbine (Bak et al. (2013)), and a commercial lidar system. The simulations are performed with a lidar simulator module added to the OpenFAST simulation tool NWTC (2018), providing the line-of-sight measurements considering the lidar system motion. Additionally, an inertial measurement unit (IMU) is simulated. First, the IMU and lidar data is processed to a motion-compensated rotor-effective wind speed (REWS). Then, the multi-variable feedforward controller uses the REWS to provide a pitch rate and a generator torque update. Finally, the feedback controller uses the feedforward signals to reduce the impact of wind changes on the wind turbine. Simulation results show that, even with a realistic wind preview, the feedforward controller is able to significantly reduce rotor speed variations as well as structural loads and platform motions.

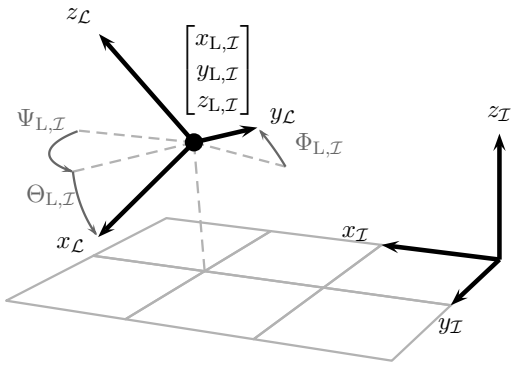

Figure 1: *Orientation of the lidar coordinate system (subscript $\mathcal{L}$) in the inertial coordinate system (subscript $\mathcal{I}$).*

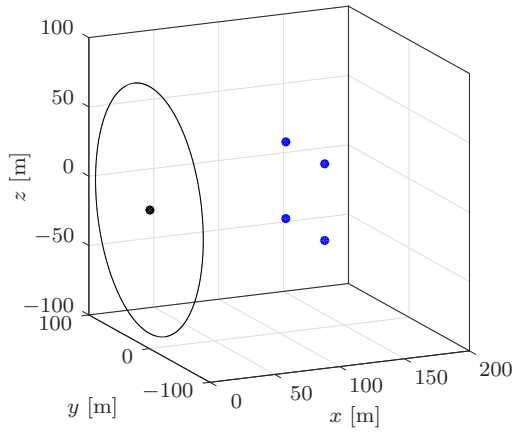

Figure 2: *Sketch of the scan pattern of the selected lidar system.*

REALISTIC SIMULATION ENVIRONMENT: OPENFAST

For a realistic dynamic simulation, the DTU 10 MW Triple Spar floating wind turbine is implemented in the coupled aero-hydro-servo-elastic simulation tool OpenFAST, which has been extended with a realistic lidar simulator. The lidar data processing and the controllers are implemented in DLL modules (sowento-DLL-Chain) and connected to the simulation via the controller DLL interface of OpenFAST. In the following the main adaptions of the simulation tool are described.

Lidar Simulator

The OpenFAST lidar simulator is an extension of OpenFAST developed at the University of Stuttgart and sowento based on (Schlipf et al., 2009), which provides raw lidar data during a turbine simulation by scanning the same wind field which is used for the aero-hydro-servo-elastic simulation.

The simulator works with uniform and Bladed-style turbulent wind. When calculating the line-of-sight wind speeds, it takes into account the motion of the nacelle to which the lidar is assumed to be attached (see Figure 1). Furthermore, volume measurements are simulated by applying an user-defined weighting function to multiple measurements near a single focal point. The lidar simulator can be configured like any other OpenFAST module by modifying an input file. The input file allows the customization of the position and orientation of the lidar on the nacelle, the measurement ranges and beam directions as well as the range weighting function. In general, a lidar system is only able to measure the component of the wind vector in the laser beam direction. Therefore, the line-of-sight wind speed v_{LOS} measured by a stationary lidar system can be modeled by a projection of the wind vector $[u_\mathcal{I}\ v_\mathcal{I}\ w_\mathcal{I}]^T$ on the normalized vector of the laser beam $[x_{\mathrm{B},\mathcal{I}} y_{\mathrm{B},\mathcal{I}} z_{\mathrm{B},\mathcal{I}}]^T$. This is mathematically equivalent to the scalar product of both vectors. If the lidar system is not fixed in the inertial frame, but moving with the velocity $[\dot{x}_{\mathrm{L},\mathcal{I}} \dot{y}_{\mathrm{L},\mathcal{I}} \dot{z}_{\mathrm{L},\mathcal{I}}]^T$, the resulting line-of-sight wind speed is

$$v_{\mathrm{LOS}} = x_{\mathrm{B},\mathcal{I}}(u_\mathcal{I} - \dot{x}_{\mathrm{L},\mathcal{I}}) + y_{\mathrm{B},\mathcal{I}}(v_\mathcal{I} - \dot{y}_{\mathrm{L},\mathcal{I}}) + z_{\mathrm{B},\mathcal{I}}(w_\mathcal{I} - \dot{z}_{\mathrm{L},\mathcal{I}}). \quad (1)$$

Further, real lidar systems measure within a probe volume. The volume measurement is modeled by a range weighting function f_{RW} depending on the distance a to the measurement point. For the pulsed lidar system considered in this work, a normalized Gaussian shape weighting function is used, following Cariou (2013) with a pulse width at half maximum of 30 m. Finally, the line-of-sight wind speed is modeled by

$$v_{\mathrm{LOS}} = \int_{-\infty}^{\infty} (x_{\mathrm{B},\mathcal{I}}(u_{a,\mathcal{I}} - \dot{x}_{\mathrm{L},\mathcal{I}}) + y_{\mathrm{B},\mathcal{I}}(u_{a,\mathcal{I}} - \dot{y}_{\mathrm{L},\mathcal{I}}) + z_{\mathrm{B},\mathcal{I}}(u_{a,\mathcal{I}} - \dot{z}_{\mathrm{L},\mathcal{I}}))\, f_{\mathrm{RW}}(a)\, \mathrm{d}a, \quad (2)$$

where $[u_{a,\mathcal{I}} v_{a,\mathcal{I}} w_{a,\mathcal{I}}]$ is the wind vector evaluated along the laser beam.

During the hydro-servo-aero-elastic simulations, the lidar simulator calculates the lidar position, velocity, and inclination based on the current values of all 6 platform modes and all 4 tower modes and their derivatives. The line-of-sight wind speeds v_{LOS} are then calculated using Equations (1) and applying Taylor's Hypothesis of Frozen Turbulence (Taylor, 1938), which assumes that turbulent wind travels with the mean wind speed from the measurement location to the rotor. Further, an Inertial measurement unit (IMU) is simulated.

Selected Lidar System

For this work, a commercial pulsed lidar system is used. The scan trajectory is illustrated in Figure 2. Table 1 summarizes the lidar configuration, including the azimuth angles of ±15° and elevation angles of ±12.5°. The lidar is able to take measurements in several vertical planes. The measurement coherence bandwidth (MCB) is calculated with a correlation model following Schlipf et al. (2015a); Simley et al. (2018). Figure 3 illustrates the optimization for single-distance lidar-assisted control. At a distance of $x = 120\,\mathrm{m}$ we achieve a maximum MCB of $k_{0.5} \approx 0.0218\,\mathrm{rad/m}$, which is why this particular distance is used for this work.

Following data is then provided to the lidar data processing line-of-sight: wind speed v_{LOS}, a flag for new measurements, the beam ID (0 to 3), the lidar velocity $[\dot{x}_{\mathrm{L},\mathcal{I}} \dot{y}_{\mathrm{L},\mathcal{I}} \dot{z}_{\mathrm{L},\mathcal{I}}]^T$ and the rotational degrees of freedom (yaw $\Psi_{\mathrm{L},\mathcal{I}}$, pitch $\Theta_{\mathrm{L},\mathcal{I}}$, and roll $\Phi_{\mathrm{L},\mathcal{I}}$, see Figure 1). The interface will be explained in the following subsection, the lidar data processing in the next section.

sowento DLL-Chain

The FAST ServoDyn module, which allows the configuration of the turbine controller, supports a single external Bladed-style controller DLL (Dynamic Link Library). To process the lidar data from the lidar simulator, one approach would be to compile a single controller, which carries out all desired steps, e.g., lidar

Table 1: *Selected scan configuration for the lidar system.*

Number of beams	4
Beam azimuth-angles	15.0°, 15.0°,−15.0°,−15.0°
Beam elevation-angles	12.5°, −12.5°, −12.5°, 12.5°
Selected measurement distance	120.0 m
Cycle scanning-time	1.0 s

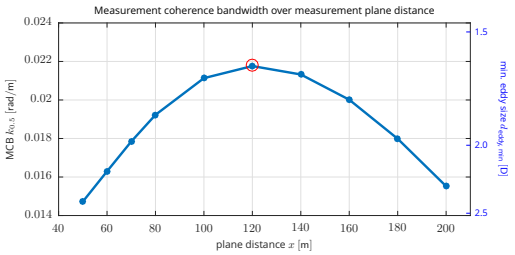

Figure 3: *Optimization of the lidar configuration.*

data-processing, feedforward control and feedback control. Here, the sowento DLL-chain is used, consisting of a master DLL, which can be configured to sequentially call multiple secondary DLLs. This allows the encapsulation of individual control steps into separate DLLs, which has several advantages:

- Individual modules can be modified by exchanging the corresponding DLL without having to recompile unrelated parts.
- Companies and institutes can share their DLLs without the need to give up confidential source code. For example, a turbine operator may share his feedback controller DLL such that a third party can combine it with a new feedforward controller, e.g., for a simulation study.
- DLLs can be loaded in a "smart lidar system". The main idea is that lidar systems need to become more interactive and more adaptive to their environment. More details can be found in Schlipf et al. (2019).
- Other functionalities (e.g. extreme event detection, lidar adaption, etc.) can easily be added in separate modules.

Figure 4 illustrates how the DLLs and the data files are connected: At every controller step, FAST calls the master DLL and passes the swap array. This array is the central part of the old Bladed interface for external controllers Bossanyi (2010). Here, the master DLL merely passes on this array to all secondary DLLs. The master DLL and every sub-DLL has its own input file, which allows the configuration of the DLL behavior. Furthermore, the master DLL writes selected signals from all DLLs to an output file. For this work, the DLL-chain consists of DLLs for lidar data-processing (LDP), feedforward control and feedback control. The LDP DLL reads the raw lidar data, which has been written into the swap array by the lidar simulator. Based on this, it calculates an estimate of the rotor-effective wind speed and stores it in the array. Next in line is the multi-variable feedforward controller, which converts the wind speed estimate into a demanded pitch rate and generator torque update signal. The feedforward control signals together with the turbine states are read by the feedback controller. This last DLL then returns the demanded torque and the demanded blade pitch angle.

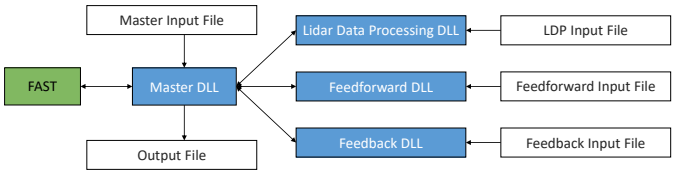

Figure 4: *Structure of the controller and data-processing DLL communication for FAST.*

CONTROLLER DESIGN MODEL: SLOW

The Simplified Low-Order Wind Turbine (SLOW) presented below was developed with the aim of a research-oriented tool, representing not more than the main dynamics for controller design and Systems Engineering applications for FOWTs. The simplification and order reduction process is important for the understanding of the design-driving physical effects, especially when it comes to canceling the wind and wave disturbance effects. Another advantage is that the computational time to set up linearized models or run time-domain simulations is reasonable. Aerodynamics and hydrodynamics are simplified to the same extent, including first-order and second-order hydrodynamics because these significantly influence the overall FOWT dynamics.

In this work the model is used to represent the effects of the transient changes of the incoming wind speed on the rotor speed, including the control inputs blade pitch θ and generator torque M_g. The rotor speed response is also influenced by the fore-aft motion of the rotor, which has its origin in the floater rigid-body dynamics and the hydrodynamic model. Having derived the SLOW model, linear state space models can be obtained to perform the controller design in the following chapter.

Modeling

For the present work, the Multibody System (MBS) has only 6 DOFs for maximum efficiency: Figure 5 shows the mechanical topology with the floating platform rigid body Degrees of Freedom (DOFs) in surge (x_p), heave (z_p) and pitch (β_p), the flexible tower with one representative coordinate (x_t), the rotor speed (Ω) and the blade pitch actuator (θ). The motion is constrained to the vertical 2D-plane, in which wind and wave forces act.

The model has proven its ability to accurately predict the FOWT response in stochastic wind and wave conditions in previous works. It was compared against scaled experiments of the TripleSpar platform in Yu et al. (2017). An extensive comparison against FAST NWTC (2018) across a range of semi-submersible floaters as well as more details about the equation of motions can be found in the dissertation Lemmer (2018). It was used for controller design previously and the control performance and robustness against unmodeled dynamics was proven through a comparison against FAST in Lemmer et al. (2016b); Yu et al. (2018).

The aerodynamic model has been simplified, compared to Blade-Element Momentum Theory, and avoids iterations to compute the lift and drag coefficients along the blade Hansen (2000). Instead, the bulk flow across the entire rotor is considered without resolving the load distribution along the blade. For this end, the rotor thrust and torque is calculated for different tip speed ratios and blade pitch angles, resulting in a look-up table that can be used in each time step by SLOW.

The hydrodynamic model shall reliably predict the forcing as well as damping properties to be accounted for by the controller.

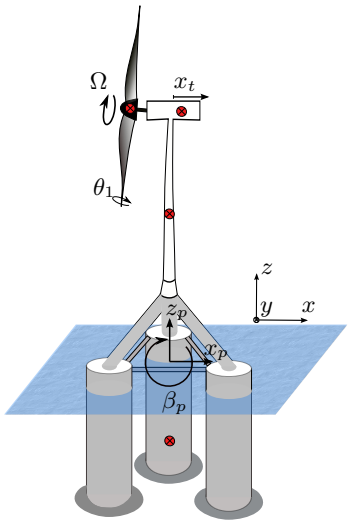

Figure 5: *Topology of the employed multi-body model Lemmer et al. (2020a).*

The first-order panel code coefficients and a node-based Morison drag model are combined for this end. For the analyzed floater shape, it is appropriate to neglect radiation damping due to the dominance of viscous effects. This gives a significant improvement of the computational efficiency through the frequency-independent added mass and the absence of a convolution integral Lemmer (2018). Newman's approximation Standing et al. (1987) introduces the low-frequency slow-drift forcing. The mooring forces are simulated by a quasi-static approach.

The nonlinear state-space equations of motion are linearized for controller design about all operating points. The aerodynamic coefficients are linearized through a tangent approximation using a central difference scheme. The quadratic Morison drag is linearized using Borgman's method Borgman (1965). It results from the standard deviation (STD) of the nodal velocity of the submerged portion of the floater.

LIDAR DATA PROCESSING

In the lidar data-processing DLL, a baseline wind field reconstruction for the lidar measurement of the 4-Beam lidar system is implemented. It obtains the line-of-sight wind speed v_{LOS}, a flag for new measurements, the beam ID (0 to 3), the lidar velocity $[\dot{x}_{\mathrm{L},\mathcal{I}}\dot{y}_{\mathrm{L},\mathcal{I}}\dot{z}_{\mathrm{L},\mathcal{I}}]^T$ and the rotational degrees of freedom from the lidar simulator via the swap array and the Master DLL and provides the rotor-effective wind speed to the multi-variable feedforward controller.

The lidar data processing consists of a coordinate transformation, the motion compensation based on the available measurements and the estimation of the rotor-effective wind speed.

Coordinate Transformation

The simulated inertial measurement unit (IMU) of the lidar provides the rotational degrees of freedom and the lidar velocity in the fixed inertial coordinates ($\mathcal{I}$), see Figure 1). In the input file of the LDP-DLL, the beam direction vector $[x_{\mathrm{B},\mathcal{L}}\, y_{\mathrm{B},\mathcal{L}}\, z_{\mathrm{B},\mathcal{L}}]^{\mathrm{T}}$ is given in lidar coordinates ($\mathcal{L}$). For the lidar-data processing, we need to bring the beam direction vector into the inertial coordinates system. This can be compute by multiplying the beam direction vector in the lidar coordinate system with the rotation matrix

$$\begin{bmatrix} x_{\mathrm{B},\mathcal{I}} \\ y_{\mathrm{B},\mathcal{I}} \\ z_{\mathrm{B},\mathcal{I}} \end{bmatrix} = R(\Psi_{\mathrm{L},\mathcal{I}}, \Theta_{\mathrm{L},\mathcal{I}}, \Phi_{\mathrm{L},\mathcal{I}}) \begin{bmatrix} x_{\mathrm{B},\mathcal{L}} \\ y_{\mathrm{B},\mathcal{L}} \\ z_{\mathrm{B},\mathcal{L}} \end{bmatrix}, \tag{3}$$

where the rotation matrix is

$$R(\Psi, \Theta, \Phi) = R_{\mathrm{yaw}}(\Psi)\, R_{\mathrm{pitch}}(\Theta)\, R_{\mathrm{roll}}(\Phi). \tag{4}$$

Full Motion Compensation

The motion compensation is a special wind field reconstruction where online measurements are taken into account. For lidar-assisted control, one can assume that the wind turbine is aligned with the main wind direction and thus $\hat{v}_{\mathcal{I}} = \hat{w}_{\mathcal{I}} = 0$. In this case, we can solve (1) for the longitudinal wind speed u which yields the estimate

$$\hat{u}_{\mathcal{I}} = \frac{v_{\mathrm{LOS}} + y_{\mathrm{B},\mathcal{I}}\dot{y}_{\mathrm{L},\mathcal{I}} + z_{\mathrm{B},\mathcal{I}}\dot{z}_{\mathrm{L},\mathcal{I}}}{x_{\mathrm{B},\mathcal{I}}} + \dot{x}_{\mathrm{L},\mathcal{I}}. \tag{5}$$

By taking into account the lidar orientation and velocity, the turbine motions are compensated. During lidar data-processing, equation (5) is applied to every line-of-sight measurement v_{LOS} to obtain the longitudinal speed $\hat{u}_{\mathcal{I}}$ in every measurement point. These intermediate results are then further processed to calculate a scalar estimate of the rotor-effective wind speed v_0.

Calculation of Rotor-Effective Wind Speed

With the estimate of the longitudinal wind speed $\hat{u}_{\mathcal{I},i}$ in every measurement point i, we can then combine every four points from a full scan at one distance to

$$v_0 = \sum_{i=1}^{4} \hat{u}_{\mathcal{I},i} \tag{6}$$

following Schlipf et al. (2012).

When more measurement distances are used, the line-of-sight wind speeds of all measurement points can be used to combine them to a more accurate estimate of the rotor-effective wind speed or to estimate wind shears and wind direction as in Raach et al. (2014a). However, this is out of the scope of this work.

In this work, the rotor-effective wind speed from Equation (6) is used either directly if perfect wind preview is assumed or with a low pass filter if realistic wind preview is assumed to cancel out all uncorrelated frequency content.

CONTROLLER DESIGN

In this section, an overview of the controller implementation is given. Then the baseline controller is briefly described. Finally, the lidar-assisted collective pitch feedforward controller is derived first for perfect and then for realistic wind preview.

Baseline Feedback Controller

The baseline controller has a standard proportional-integral (PI)-layout as shown in Figure 6. It receives the generator speed error $\Omega_g - \Omega_{g,ref}$ as measurement and outputs the blade pitch angle. The design procedure resulting in the PI-gains of the controller, namely proportional gain k_p and integral gain $K_I = kp/T_i$ with time constant T_i differs from the common design procedures for onshore turbines, see Lemmer et al. (2020b).

For FOWTs, the above-rated controller introduces a negative damping, or potential instability, as mentioned in the introduction. While this substantial limitation for controller design exists also for onshore turbines, it is more critical for FOWTs because the rotor fore-aft eigenfrequency is significantly lower for FOWTs

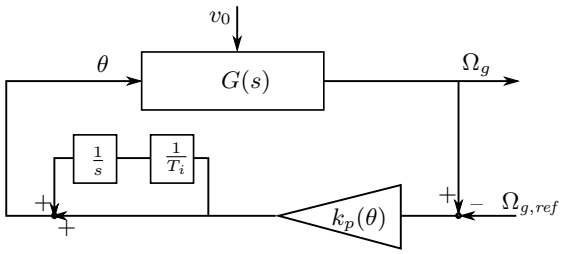

Figure 6: *PI-controller for above-rated wind speeds.*

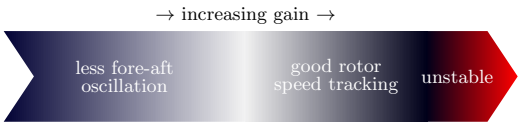

Figure 7: *Design trade-off of the PI-controller of a FOWT with negative fore-aft damping properties, from Lemmer et al. (2020b).*

because of the floating foundation. The control design limitation can be described through a main constraint on the gain magnitude (k_p and K_I), or the "aggressiveness" of the controller. The gain magnitude mainly determines the rotor speed (and therefore power) tracking properties. The better the tracking properties, the smaller is the maximum deviation of the rotor speed from the desired set point

The arrow of Figure 7 visualizes the design issue: with low gains (left part), the tracking performance is poor. With higher gains, it improves, but the controller affects more and more the fore-aft mode excitation, increasing the tower loads. If the gain is increased even further, the system can get unstable, meaning that the fore-aft eigenmode gets a positive real part.

The controller used in the current research has the gain scheduling of k_p and a constant $T_i = 9.5\,\mathrm{s}$, more details can be found in Lemmer et al. (2020b). The underlying mathematical model for determining the stability and the rotor speed mode natural frequency is the coupled reduced-order model SLOW. The main objective in the design is to find the best trade-off, as introduced in Figure 7. This best trade-off is mainly determined by the stability, which is a critical requirement in the design. Therefore, the gain k_p is found with the requirement of the system in closed loop with the controller, satisfying a stability margin of $1/M_s = 0.4$, where the maximum sensitivity M_s is an indicator comparable to the Gain Margin (GM) or Phase Margin (PM), see (Åström and Murray, 2016, p. 13-6).

Multi-Variable Feedforward Controller Design

The multi-variable feedforward controller is designed using a linear model from the SLOW model described above. Here, the gain for the collective pitch is calculated to cancel out all effects of wind changes to the tower motion. The gain for the generator torque is then calculated by compensating the impact of the wind changes and the collective pitch angle on the aerodynamic torque and thus reduces the rotor motion.

The linear model for the operation point at 16 m/s is used with the state vector x and the control and disturbance inputs u and d, respectively

$$\dot{x} = Ax + B_u u + B_d d, \tag{7}$$

where the state vector is $x = [q, \dot{q}]^T$, with $q = [x_p, z_p, \beta_p, \varphi, x_t, \theta_1]$. The dynamic matrix is A, the control input matrix is B_u and the disturbance input matrix B_d. The control input $u = [M_g, \theta]^T$ includes demanded generator torque M_g and collective pitch angle demand θ.

The disturbance input in the present model includes rotor-effective wind speed v_0 and the generalized wave forces on the platform in surge, heave and pitch.

$$d = [v_0, F_{p,x}, F_{p,z}, F_{p,\beta}]^T. \tag{8}$$

In a first step, the necessary pitch action is calculated to cancel out all effects of wind changes to the tower motion. Since the pitch angle demand θ propagates through the pitch actuator and since we have a preview based on our lidar measurements, we can directly use the pitch angle position θ_1. Thus, the gain g_1 is obtained from the equation:

$$\ddot{x}_t = \dot{x}_{11} = 0. \tag{9}$$

With $\theta_1 = x_6$ and $v_0 = d_1$ and the corresponding entries from A, B_u, and B_d, this yields

$$g_1 = -\frac{b_{d,11,1}}{a_{11,6}}. \tag{10}$$

In a second step, the necessary torque action is calculated compensating the impact of the wind changes and the collective pitch angle on rotor motion. Thus, the gain g_2 is obtained from the equation:

$$\ddot{\varphi} = \dot{\Omega} = \dot{x}_{10} = 0. \tag{11}$$

With $M_g = u_1$, this yields

$$g_2 = -\frac{b_{d,10,1} + a_{10,6} g_1}{b_{u,10,1}}. \tag{12}$$

Since the feedforward controller is based on the wind signal alone and dues not include any unstable dynamics, the combined feedback-feedforward controller is stable, if the feedback controller has been stable before. In the case of the pitch controller, g_1 can be simply applied to the derivative of the wind speed and then added to the integrator of the PI controller. In case of the torque controller implemented as a nonlinear state feedback controller, we need a zero-mean signal in form of a torque update for g_2. Thus, a high pass filter has to be used to remove the static values and to be able to adjust to changing wind conditions. Here, a cut-in frequency of $f_{\mathrm{cutin}} = 0.005\,\mathrm{Hz}$ has been used as a compromise between load reduction and generator torque activity, and thus f_{cutin} is the only tuning parameter of the feedforward controller. The cut-off frequency for the rotor-effective wind speed is chosen to $f_{\mathrm{cutoff}} = 0.05\,\mathrm{Hz}$ based on the cut-off wave number from the lidar scan optimization.

The buffer time $T_{\mathrm{Buffer},2}$ for simulations with perfect wind preview is obtained by the measurement distance 120 m divided by the mean wind speed 16 m/s, since the generator torque is able to react instantaneous. For the buffer time in the pitch rate feedforward path, $T_{\mathrm{Buffer},1}$ is reduced by 0.3 s to account for the pitch actuator delay. For simulations with realistic wind preview, both buffer times are reduced by 3 s to account for the delay by the filters.

SIMULATION RESULTS

In this section, first the lidar data processing is evaluated. Then, the multi-variable feedforward controller is evaluated by simulations using perfect wind preview and simulated lidar measurements.

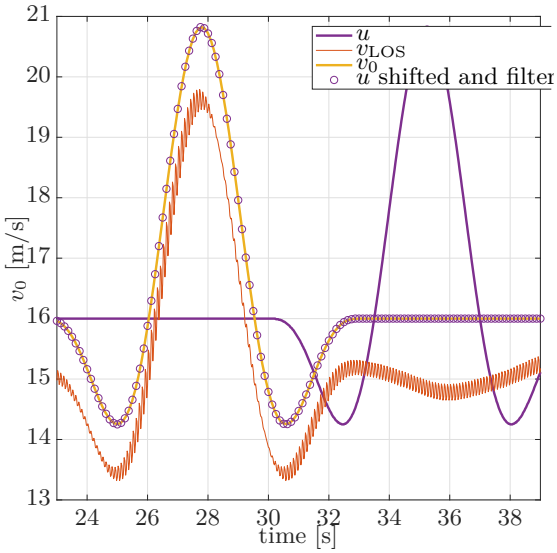

Figure 8: *Results of motion compensation test simulation.*

Simulations to Evaluate Motion Compensation

In our first simulation study, the full motion compensation is tested with for an Extreme Operating Gust (EOG) at 16 m/s according to the IEC 61400-1 (2005) using the feedback controller only. For this test, the time between each measurements is set to the simulation time step (0.025 s). The advantage here is that one can easily calculate what should be the expected lidar estimate of the rotor-effective wind speed under full motion compensation: the EOG is shifted by 7.5 s based on Taylor's Frozen Turbulence Hypothesis using a mean wind speed of 16 m/s and a measurement distance of 120 m) and then filtered by a moving average of 4 samples. Figure 8 shows that due to the line-of-sight wind speed v_{LOS} is disturbed by the motion of the lidar. However, the reconstructed and motion compensated rotor-effective wind speed v_0 fits perfectly to the expectations. This successfully evaluates the motion compensation.

Simulations Using Perfect Wind Preview and Still Sea

In second simulation study, the multi-variable feedforward controller is tested with an extreme operating gust and no waves. For this purpose, the full aero-hydro-servo-elastic model is disturbed by an EOG at 16 m/s again. The proposed feedforward controller can achieve almost perfect cancellation of the effect from v_0 to Ω, see Figure 9. The overshoot of the rotor speed (deviation from $\Omega_{\mathrm{rated}} = 9.6$ rpm) can be reduced by 98.5 %, the maximum deviation from the static platform pitch angle β_P by 90.1 %, and the maximum tower base fore-aft bending moment M_{yT} by 32.9 % compared to the feedback controller, see Table 2.

The proposed feedforward controller demonstrates a good robustness against model uncertainties. Although the controller is designed with a linear model with only 6 DOFs, it is able to almost perfectly cancel out the effect from the rotor-effective wind to the rotor speed for a full aero-hydro-servo-elastic model with 22 DOFs over a large range of wind speeds.

This yields also less oscillation in the turbine and platform structure, such as the tower top displacement x_t and the platform displacement x_p.

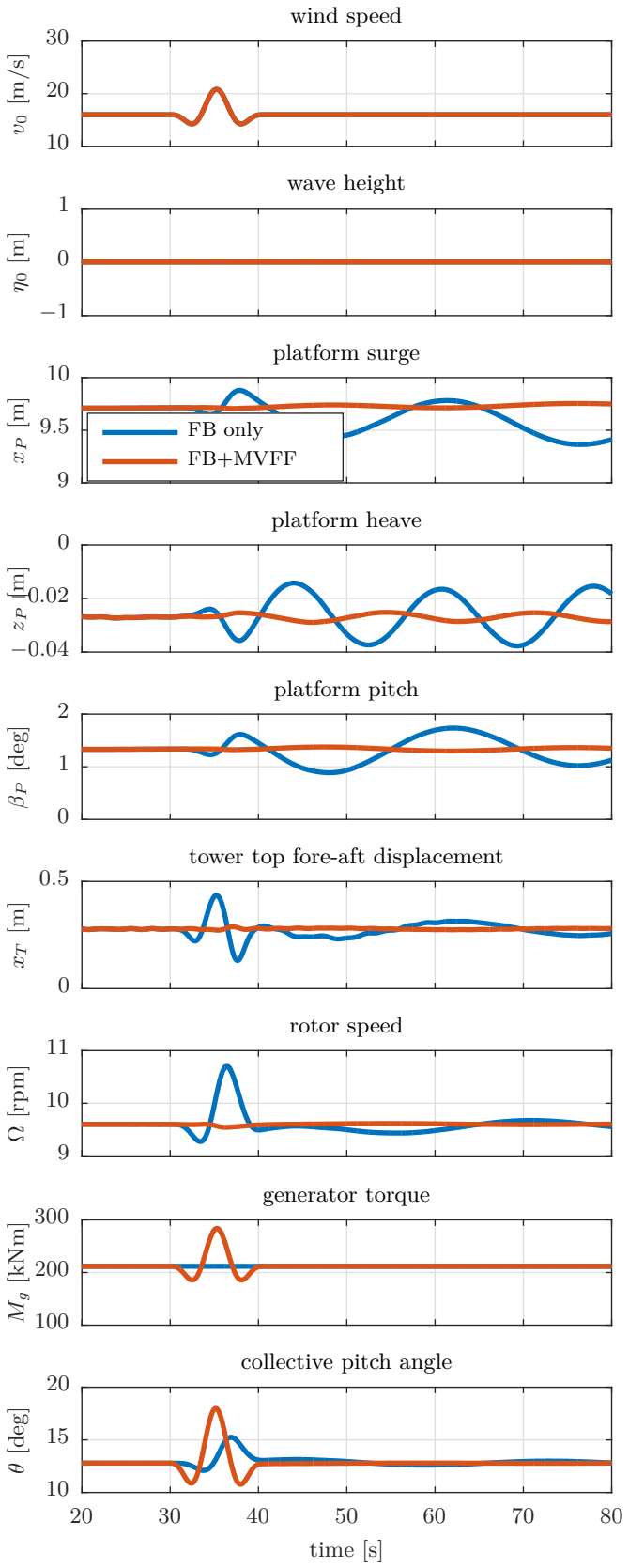

Figure 9: *Time comparison of feedback only and combined feedback with multi-variable feedforward controller for coherent wind and no waves.*

Table 2: *Maximum values of the simulation with an EOG at* 16 m/s *with perfect wind preview (see Figure 9).*

	FB	FB+FF	$\frac{\text{FB+FF}}{\text{FB}}$ [%]
$\Delta\Omega$ [rpm]	1.100	0.016	1.5
$\Delta\beta_P$ [deg]	0.445	0.044	9.9
M_{yT} [MNm]	138.3	94.2	68.1

Table 3: *Comparison of the results for the* 1 h *simulation at* 18 m/s *using feedback (FB) and using feedback and feedforward control (FB+FF).*

	FB	FB+FF	$\frac{\text{FB+FF}}{\text{FB}}$ [%]
DEL(M_{yT}) [MNm]	320.5	292.3	91.2
DEL(M_{oop1}) [MNm]	19.90	14.67	73.7
STD(Ω) [rpm]	0.567	0.157	27.7
STD(x_p) [m]	2.105	1.507	71.6
STD(β_P) [deg]	0.679	0.284	41.8

Simulations Using Realistic Wind Preview and Waves

In a third simulation study, the robustness against lidar wind preview measurement errors is examined. For this investigation, a turbulent wind field with turbulence class "A" according to (IEC 61400-1, 2005), resulting in a turbulence intensity of 17.6 % and a length of over 1 h is generated with TurbSim with a mean wind speed of $\bar{u} = 16$ m/s. The width and height of the wind field are each 208 m and the resolution is 8 m, resulting in 27×27 grid points. The temporal resolution is 0.25 s. With this wind field, the full aero-hydro-servo-elastic model is simulated for 3600 s. All states are initialized with their steady values corresponding to the rotor-effective wind speed (average over the rotor disk) at the beginning of the simulation. During simulations, the wind field is scanned by the lidar simulator taking into account the current position, velocity, and inclination of the lidar system. From the raw lidar data, the rotor-effective wind speed is reconstructed and filtered as described above. Additionally, the floating wind turbine is disturbed by irregular waves of significant wave height H_s=3.7 m, and peak spectral period T_p=9.8 s with a JONSWAP spectrum.

Figure 10 illustrates a representative 10 min period of the simulation. With the realistic lidar wind preview, the variation in the rotor speed Ω is still reduced significantly. Additionally, the variation in platform displacement x_p, platform pitch β_P, the tower top displacement x_t, and the resulting tower base fore-aft bending moment M_{yT} are reduced.

Table 3 summarizes the results of the 1 h simulation at 16 m/s. For the calculation of the Damage Equivalent Loads (DELs), a reference number of cycles $n_{ref} = 2 \times 10^6$ is used. Further, a Wöhler exponent of $m = 4$ is assumed for the fatigue load calculation of the tower base fore-aft bending moment M_{yT}. For M_{oop1}, the out-of-plane blade root bending moment of blade 1, a Wöhler exponent of $m = 10$ is applied. Besides the above-mentioned load reduction on the tower base of almost 19 %, additional load reduction on blade root of over 25 % is achieved. This is mainly because the standard deviation (STD) of the platform pitch angle β_P can be reduced by over 50 % and of the platform surge x_p by almost 30 %. Over 70 % reduction in the standard deviation of the rotor speed can be achieved.

These results confirm that multi-variable pitch feedforward control is very promising for FOWTs even considering wind preview measurement uncertainties.

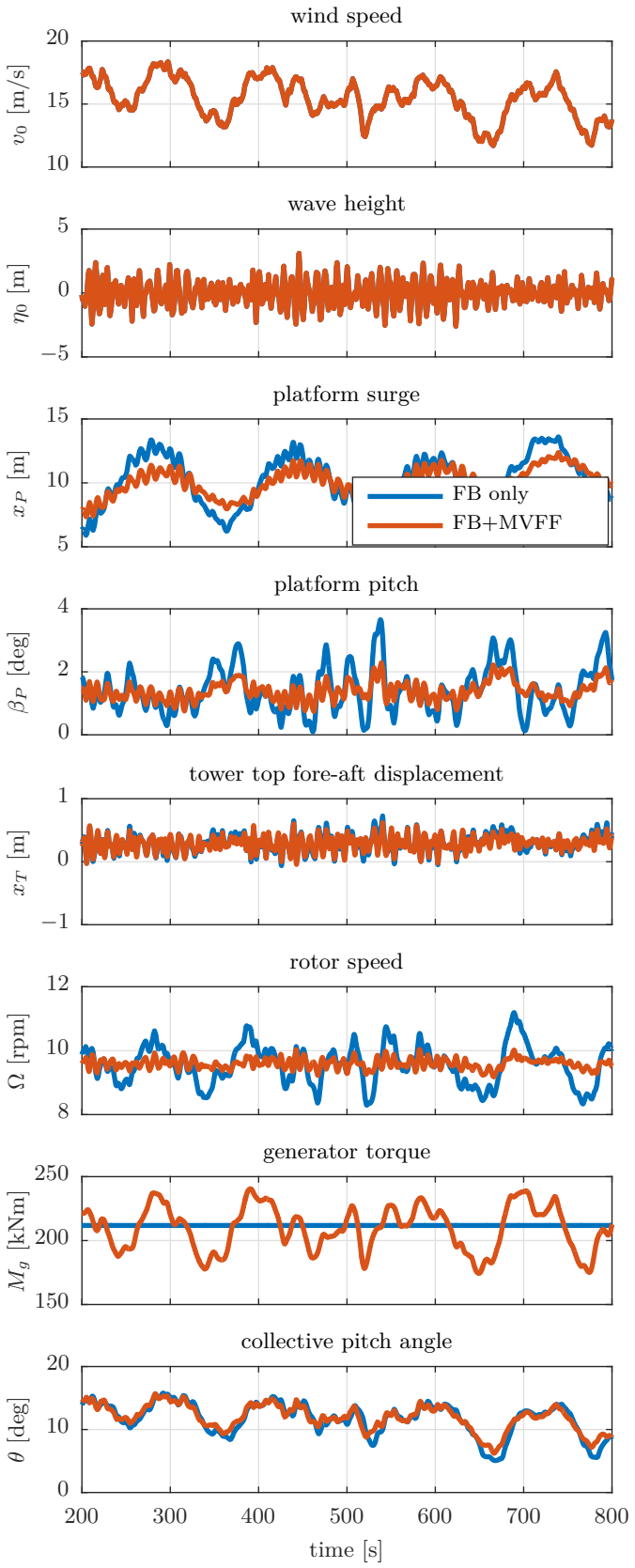

Figure 10: *Time comparison of feedback only and combined feedback with multi-variable feedforward controller for turbulent wind and irregular waves.*

CONCLUSIONS AND OUTLOOK

In this work, we presented a multi-variable feedforward controller which is able to use both collective pitch and generator torque feedforward control. The approach is very promising for floating wind turbines, since for a large frequency band, the impact of wind speed changes on aerodynamic torque and thrust can be compensated which reduces the platform motion while keeping the rotor speed close to the rated value.

The simulation results show that with perfect preview, rotor and tower as well as platform motion can be hold almost constant. For realistic wind preview based on a realistic lidar simulator, a reduction in rotor, tower and platform motion is clearly visible. The lidar data processing and the feedback and feedforward controller are implemented in modular, compiled form such that a commercial implementation is facilitated.

In future work we will test parts of the approach on a commercial floating wind turbine. We will further investigate, how the wave preview e.g. by wave radar systems can be used to additionally reduce the loads at the wave spectrum frequencies. This might involve a more sophisticated platform design and additional actuators.

ACKNOWLEDGEMENTS

A planned prototype test campaign of the presented controller will take place in the German-French research project VAMOS. It is funded by the German Federal Ministry for Economic Affairs and Energy (BMWi) and Projektträger Jülich (PTJ). Support is greatly acknowledged.

References

Al, MK (2019). *Feedforward control for wave disturbance rejection on floating offshore wind turbines*, Msc thesis, TU Delft.

Åström, KJ and Murray, RM (2016). *Feedback Systems*, Princeton University Press, 2nd edition.

Bak, C, Zahle, F, Bitsche, R, Kim, T, Yde, A, Henriksen, L, Natarajan, A, and Hansen, M (2013). "Description of the DTU 10MW reference wind turbine," Technical report, Technical University of Denmark, Roskilde, Denmark.

Borgman, LE (1965). "The spectral density for ocean wave forces," in *Proceedings of the Santa Barbara Coastal Engineering Conference*, pages 147–182, Santa Barbara, USA.

Bossanyi, E (2010). *GH Bladed Version 3.85 User Manual*.

Cariou, JP (2013). "Pulsed lidars," in *Remote Sensing for Wind Energy, DTU Wind Energy-E-Report-0029(EN)*, chapter 5, pages 104–121.

Hansen, MOL (2000). *Aerodynamics of Wind Turbines*, Earthscan, 2nd edition.

IEC 61400-1 (2005). "Wind turbines - Part 1: Design requirements," .

Lemmer, F (2018). *Low-Order Modeling, Controller Design and Optimization of Floating Offshore Wind Turbines*, Ph.D. thesis, University of Stuttgart.

Lemmer, F, Raach, S, Schlipf, D, and Cheng, PW (2016a). "Parametric wave excitation model for floating wind turbines," *Energy Procedia*, volume 94, pages 290–305.

Lemmer, F, Raach, S, Schlipf, D, Faerron-Guzmán, R, and Cheng, PW (2020a). "FAST model of the SWE-TripleSpar floating wind turbine platform for the DTU 10MW reference wind turbine," Technical report, University of Stuttgart - SWE, https://dx.doi.org/10.18419/darus-514.

Lemmer, F, Schlipf, D, and Cheng, PW (2016b). "Control design methods for floating wind turbines for optimal disturbance rejection," *Journal of Physics: Conference Series*, volume 753, page 092006.

Lemmer, F, Yu, W, Schlipf, D, and Cheng, PW (2020b). "Robust gain scheduling baseline controller for floating offshore wind turbines," *Wind Energy*, volume 23(1).

NWTC (2018). "NWTC Information Portal (OpenFAST)," .

Raach, S, Schlipf, D, Haizmann, F, and Cheng, PW (2014a). "Three dimensional dynamic model based wind field reconstruction from lidar data," *Journal of Physics: Conference Series*, volume 524(1), page 012005.

Raach, S, Schlipf, D, Sandner, F, Matha, D, and Cheng, PW (2014b). "Nonlinear model predictive control of floating wind turbines with individual pitch control," in *Proceedings of the American Control Conference*, pages 4434–4439, Portland, Oregon, USA.

Schlipf, D, Haizmann, F, Cosack, N, Siebers, T, and Cheng, PW (2015a). "Detection of wind evolution and lidar trajectory optimization for lidar-assisted wind turbine control," *Meteorologische Zeitschrift*, volume 24(6), pages 565–579.

Schlipf, D, Raach, S, Koch, M, and Fu, W (2019). "The smart lidar idea," Technical report, sowento GmbH, https://www.sowento.com/sowentos-smart-lidar-framework/.

Schlipf, D, Rettenmeier, A, Haizmann, F, Hofsäß, M, Courtney, M, and Cheng, PW (2012). "Model based wind vector field reconstruction from lidar data," in *Proceedings of the German Wind Energy Conference DEWEK*, Bremen, Germany.

Schlipf, D, Schlipf, DJ, and Kühn, M (2013). "Nonlinear model predictive control of wind turbines using LIDAR," *Wind Energy*, volume 16(7), pages 1107–1129.

Schlipf, D, Simley, E, Lemmer, F, Pao, L, and Cheng, PW (2015b). "Collective pitch feedforward control of floating wind turbines using LIDAR," *Journal of Ocean and Wind Energy*, volume 2(4), pages 440–447.

Schlipf, D, Trujillo, JJ, Basterra, V, and Kühn, M (2009). "Development of a wind turbine LIDAR simulator," in *Proceedings of the European Wind Energy Conference*, Marseille, France.

Simley, E, Fürst, H, Haizmann, F, and Schlipf, D (2018). "Optimizing lidars for wind turbine control applications – results from the iea wind task 32 workshop," *Remote Sensing*, volume 10(863).

Standing, R, Brendling, W, and Wilson, D (1987). "Recent developments in the analysis of wave drift forces, low-frequency damping and response," in *Proceedings of the Offshore Technology Conference*, Houston, USA.

Taylor, GI (1938). "The spectrum of turbulence," *Proceedings of the Royal Society of London. Series A - Mathematical and Physical Sciences*, volume 164(919), pages 476–490.

Yu, W, Lemmer, F, Bredmose, H, Borg, M, Pegalajar-Jurado, A, Mikkelsen, RF, Stoklund Larsen, T, Fjelstrup, T, Lomholt, A, Boehm, L, Schlipf, D, and Azcona, J (2017). "The TripleSpar Campaign: Implementation and test of a blade pitch controller on a scaled floating wind turbine model," in *Energy Procedia*, volume 137, pages 323–338, Elsevier, Trondheim, Norway.

Yu, W, Lemmer, F, Schlipf, D, Cheng, PW, Visser, B, Links, H, Gupta, N, Dankelmann, S, Couñago, B, and Serna, J (2018). "Evaluation of control methods for floating offshore wind turbines," volume 1104, page 012033, IOP Publishing.